Pergamon

Acta mater. Vol. 45, No. 9, pp. 3687–3694, 1997

Printed in Great Britain
PII: S1359-6454(97)00067-0
1359-6454/97 $17.00 + 0.00

A SELF-CONSISTENT APPROACH FOR MODELLING TEXTURE DEVELOPMENT OF TWO-PHASE POLYCRYSTALS: APPLICATION TO TITANIUM ALLOYS

R. A. LEBENSOHN[1] and G. R. CANOVA[2]

[1]IFIR (UNR-CONICET), Bv. 27 de Febrero 210 Bis, 2000 Rosario, Argentina and [2]GPM2, ENSPG, Domaine Universitaire, BP 46, 38402 St Martin d'Heres Cedex, France

(Received 25 September 1996; accepted 3 January 1997)

Abstract—A large strain self-consistent viscoplastic model is proposed, developed and applied to a two-phase polycrystal. This model accounts for crystallographic textures and grain morphologies, as well as for the phase correlation, both in space and orientation. The basic formulation is shown and the case of lamellar ($\alpha + \beta$) Ti alloys in rolling is studied. In these alloys, the two phases exhibit specific morphologic and crystallographic correlations. The present study shows that the model leads to better texture predictions when all these correlations are accounted for. © *1997 Acta Metallurgica Inc.*

1. INTRODUCTION

Due to the increasing complexity of the materials used for engineering applications, more sophisticated models need to be developed. In the past, the main source of anisotropy of polycrystals was considered to be due to crystallographic textures and the well known Sachs [1] and Taylor [2] models were developed mainly to account for these effects. The latter has been quite successful for single-phase materials exhibiting a not too large crystal anisotropy, such as high SFE cubic metals. For crystals of higher anisotropy, like the ones having hexagonal symmetry, somewhat more complex models are required, e.g. self-consistent models, such as the one developed by Hutchinson [3] in the small strain elastic–plastic context. In some cases, viscosity effects are quite important and a rate-sensitive approach must be used, which can also be done in the framework of viscoplastic self-consistent (VPSC) models [4–6]. These VPSC models can be formulated either in terms of the general Zeller–Dederichs approach [7] (as in Ref. [5]) or the more restricted (but completely equivalent) Eshelby–Hill approach [8, 9] (as in Refs [4] and [6]). When grains become heavily distorted their morphology can affect their mechanical response and the Relaxed Constraints approach [10, 11] can be used, which is rigorous as a limit of infinitely flat grains. These effects can also be introduced within self-consistent schemes as shown by Tiem *et al.* [12], and this has been done extensively in many applications.

When different phases are present in the material, then their spatial distribution can be of some importance, and different types of modelling can be developed depending on that distribution. The model proposed by Molinari *et al.* [5], in its general n-sites formulation, is an adequate framework for this case. Canova *et al.* [13] implemented this n-sites approach for the calculation of texture development of a quartz–mica aggregate. In doing this, they divided a representative set of grains into small cubes, in such a way that each grain contains several cubes and each cube has the properties of the grain where it is located. Then, they accounted for the interaction of each cube with their 26 neighbours, all of them embedded in a Homogeneous Equivalent Medium (HEM) with average properties over the complete set of cubes. There are, however, many cases of two-phase polycrystals for which the vicinity effect between phases is mainly due to a strong correlation in orientation and morphology between neighbour regions of both phases. Furthermore, as the regions of both phases usually form a stack, this correlation is periodically repeated. Therefore, the proper way to account for the effect of this correlation is to consider two interacting regions of different phases deforming in the HEM.

Good examples of these "correlated" two-phase materials are the lamellar ($\alpha + \beta$) Ti alloys. In these alloys, the regions corresponding to one phase are rather flat, and each region of a given phase is always a neighbour to a region of the other phase. Their crystallographic orientation is also subjected to certain rules described by the Burgers relation that puts one given crystallographic line and plane of one grain in coincidence with another plane and line of the other grain. The large strain rolling texture of these alloys has not been explained yet by any model, and here we propose a solution to it.

In the following section, the model will be firstly explained and then developed. In doing this, we

choose to use Eshelby–Hill formalism (rather than the Zeller–Dederichs one) and, therefore, we will extend the one-inclusion problem to the case of two interacting ellipsoidal inclusions. An application will be presented afterwards for the $(\alpha+\beta)$ Ti alloys, accounting for an increasing number of microstructural features, e.g. texture, grain morphologies, spatial correlation and orientation correlation between phases.

2. MODEL

2.1. Notation

In what follows, scalars are denoted by italic letters, vectors (without subindices) are bold-face letters, second-order tensors are bold-face letters underlined once and fourth-order tensors are bold-face letters underlined twice. Tensorial and twice contracted products are denoted by "$\otimes$" and ":", respectively. For example:

$$\mathbf{C} = \underline{\mathbf{A}} \otimes \underline{\mathbf{B}} \Leftrightarrow C_{ijkl} = A_{ij}B_{kl} \tag{1a}$$

$$C = \underline{\mathbf{A}}:\underline{\mathbf{B}} \Leftrightarrow C = A_{ij}B_{ij} \tag{1b}$$

Square brackets are used for matrices without subindices (e.g.: $[A]$).

2.2. The two-inclusions problem

Eshelby's solution for the one-inclusion problem [8, 14] is extended here to the case of two interacting ellipsoidal inclusions (#1 and #2) with eigen-strains $\underline{\boldsymbol{\epsilon}}^{1*}$ and $\underline{\boldsymbol{\epsilon}}^{2*}$, respectively, embedded in a matrix which undergoes a macroscopic stress–strain state $(\underline{\boldsymbol{\Sigma}}, \underline{\mathbf{E}})$. If $(\underline{\boldsymbol{\sigma}}^1, \underline{\boldsymbol{\epsilon}}^1)$ and $(\underline{\boldsymbol{\sigma}}^2, \underline{\boldsymbol{\epsilon}}^2)$ are the local states, the stress and strain deviations are written as:

$$\underline{\tilde{\boldsymbol{\sigma}}}^1 = \underline{\boldsymbol{\sigma}}^1 - \underline{\boldsymbol{\Sigma}} \tag{2a}$$

$$\underline{\tilde{\boldsymbol{\sigma}}}^2 = \underline{\boldsymbol{\sigma}}^2 - \underline{\boldsymbol{\Sigma}} \tag{2b}$$

$$\underline{\tilde{\boldsymbol{\epsilon}}}^1 = \underline{\boldsymbol{\epsilon}}^1 - \underline{\mathbf{E}} \tag{2c}$$

$$\underline{\tilde{\boldsymbol{\epsilon}}}^2 = \underline{\boldsymbol{\epsilon}}^2 - \underline{\mathbf{E}}. \tag{2d}$$

The strain deviations and eigen-strains are related according to the following extended Eshelby's relations:

$$\underline{\tilde{\boldsymbol{\epsilon}}}^1 = \mathbf{S}^{11}:\underline{\boldsymbol{\epsilon}}^{1*} + \mathbf{S}^{12}:\underline{\boldsymbol{\epsilon}}^{2*} \tag{3a}$$

$$\underline{\tilde{\boldsymbol{\epsilon}}}^2 = \mathbf{S}^{21}:\underline{\boldsymbol{\epsilon}}^{1*} + \mathbf{S}^{22}:\underline{\boldsymbol{\epsilon}}^{2*} \tag{3b}$$

where:

(a) $\mathbf{S}^{11}$ and $\mathbf{S}^{22}$ are the ordinary Eshelby tensors for inclusions #1 and #2, respectively. For an ellipsoidal inclusion, the Eshelby tensor depends on the properties of the homogeneous medium and the shape of the ellipsoid;

(b) $\mathbf{S}^{12}$ and $\mathbf{S}^{21}$ will be naturally designed as 2-site Eshelby tensors, i.e. the coupling factors between the eigen-strain in one inclusion and the local deviation in strain of the other one.

A general expression for Eshelby tensors is given by (α and β being 1 or 2):

$$\mathbf{S}^{\alpha\beta} = \mathrm{sym}(\boldsymbol{\Gamma}^{\alpha\beta}):\mathbf{L} \tag{4}$$

where $\mathbf{L}$ is the stiffness of the medium. For $\alpha = \beta$, $\boldsymbol{\Gamma}^{\alpha\alpha}$ depends on $\mathbf{L}$ and on the shape of the ellipsoid. For $\alpha \neq \beta$, $\boldsymbol{\Gamma}^{\alpha\beta}$ also depends on the relative orientation, relative distance and relative volume of the ellipsoids. The integrals for the calculation of $\boldsymbol{\Gamma}^{\alpha\beta}$ can be deduced from Berveiller *et al.* [15] and are given in the Appendix.

Inverting equations (3) we get:

$$\underline{\boldsymbol{\epsilon}}^{1*} = \mathbf{T}^1:\mathbf{U}^1:\underline{\tilde{\boldsymbol{\epsilon}}}^1 - \mathbf{T}^1:\underline{\tilde{\boldsymbol{\epsilon}}}^2 \tag{5a}$$

$$\underline{\boldsymbol{\epsilon}}^{2*} = -\mathbf{T}^2:\underline{\tilde{\boldsymbol{\epsilon}}}^1 + \mathbf{T}^2:\mathbf{U}^2:\underline{\tilde{\boldsymbol{\epsilon}}}^2 \tag{5b}$$

where:

$$\mathbf{T}^1 = (\mathbf{S}^{22}:[\mathbf{S}^{12}]^{-1}:\mathbf{S}^{11} - \mathbf{S}^{21})^{-1} \tag{6a}$$

$$\mathbf{U}^1 = \mathbf{S}^{22}:[\mathbf{S}^{12}]^{-1} \tag{6b}$$

and where $\mathbf{T}^2$ and $\mathbf{U}^2$ can be obtained interchanging indexes 1 and 2 in equations (6).

2.3. Viscoplastic self-consistent model

The secant viscoplastic constitutive relation between the strain-rate $\dot{\underline{\boldsymbol{\epsilon}}}$ and the stress $\underline{\boldsymbol{\sigma}}$, for a single crystal with different active slip systems is given by [4, 6]:

$$\dot{\underline{\boldsymbol{\epsilon}}} = \left\{ \dot{\gamma}_o \sum_s \frac{\underline{\underline{\mathbf{m}}}^s \otimes \underline{\underline{\mathbf{m}}}^s}{\tau_o^s} \left(\frac{\underline{\underline{\mathbf{m}}}^s:\underline{\boldsymbol{\sigma}}}{\tau_o^s} \right)^{n-1} \right\}:\underline{\boldsymbol{\sigma}} = \mathbf{M}_c^{(sec)}(\underline{\boldsymbol{\sigma}}):\underline{\boldsymbol{\sigma}} \tag{7}$$

where $\underline{\underline{\mathbf{m}}}^s$ is the Schmid tensor which expresses the orientation of the slip system (s) in crystal axes, $\dot{\gamma}_o$ is a reference rate, τ_o^s is a threshold stress which can be identified with the critical resolved shear stress (CRSS) of the slip system and n is the inverse of the rate sensitivity. The sum runs over the complete set of active slip systems. $\mathbf{M}_c^{(sec)}$ is the secant viscoplastic compliance modulus. The tangent constitutive equation can be expressed as:

$$\dot{\underline{\boldsymbol{\epsilon}}} = \left.\frac{\partial \dot{\underline{\boldsymbol{\epsilon}}}}{\partial \underline{\boldsymbol{\sigma}}}\right|_{\underline{\boldsymbol{\sigma}}} :\underline{\boldsymbol{\sigma}} + \dot{\underline{\boldsymbol{\epsilon}}}^o = \mathbf{M}_c^{(tg)}(\underline{\boldsymbol{\sigma}}):\underline{\boldsymbol{\sigma}} + \dot{\underline{\boldsymbol{\epsilon}}}^o(\underline{\boldsymbol{\sigma}}) \tag{8}$$

where $\mathbf{M}_c^{(tg)}$ is the tangent viscoplastic modulus and $\dot{\underline{\boldsymbol{\epsilon}}}^o$ is a back extrapolated term. $\mathbf{M}_c^{(sec)}$ and $\mathbf{M}_c^{(tg)}$ are related by:

$$\mathbf{M}_c^{(tg)} = n\mathbf{M}_c^{(sec)}. \tag{9}$$

The secant and tangent constitutive relations and the secant–tangent connection for a polycrystal formed by grains with local properties described by equations (7)–(9) which undergoes a macroscopic

stress–strain rate ($\underline{\dot{E}}$, $\underline{\Sigma}$) are formally equivalent to the microscopic ones [4, 6]:

$$\underline{\dot{E}} = \mathbf{M}^{(sec)}(\underline{\Sigma}):\underline{\Sigma} \tag{10}$$

$$\underline{\dot{E}} = \mathbf{M}^{(tg)}(\underline{\Sigma}):\underline{\Sigma} + \underline{\dot{E}}^{o}(\underline{\Sigma}) \tag{11}$$

$$\mathbf{M}^{(tg)} = n\mathbf{M}^{(sec)}. \tag{12}$$

Due to the extremely simple secant–tangent connection, both at micro- and macro-levels [i.e. equations (9) and (12)], we can write the equations of the VPSC model—which is essentially a *tangent formulation*—in terms of either the secant or the tangent moduli.

A two-phase polycrystal is regarded as an aggregate of pairs of sites. Each site can be a grain or a representative region inside a grain. The local behaviour is described by equations (7)–(9). The 2-site viscoplastic self-consistent (VPSC-2S) model consists of solving the problem of each pair of sites considered as two viscoplastic inhomogeneities embedded in a HEM which has the average properties of the polycrystal. This problem can be readily solved replacing the inhomogeneities by equivalent inclusions with appropriate eigen-strain rates $\underline{\dot{\epsilon}}^{1*}$ and $\underline{\dot{\epsilon}}^{2*}$ [14]. For this equivalent two-inclusions problem, the relations derived in the former section still hold, considering the strain-rate (instead of the strain) as state variable. It can be easily demonstrated [6] that the local deviations in stress and strain-rate are related by:

$$\underline{\tilde{\dot{\epsilon}}}^{1} - \underline{\dot{\epsilon}}^{1*} = \mathbf{M}^{(tg)}:\underline{\tilde{\sigma}}^{1} \tag{13a}$$

$$\underline{\tilde{\dot{\epsilon}}}^{2} - \underline{\dot{\epsilon}}^{2*} = \mathbf{M}^{(tg)}:\underline{\tilde{\sigma}}^{2} \tag{13b}$$

Replacing equations (5) in (13) we get a pair of *interaction equations*:

$$\underline{\tilde{\dot{\epsilon}}}^{1} = -\tilde{\mathbf{M}}^{11}:\underline{\tilde{\sigma}}^{1} - \tilde{\mathbf{M}}^{12}:\underline{\tilde{\sigma}}^{2} \tag{14a}$$

$$\underline{\tilde{\dot{\epsilon}}}^{2} = -\tilde{\mathbf{M}}^{21}:\underline{\tilde{\sigma}}^{1} - \tilde{\mathbf{M}}^{22}:\underline{\tilde{\sigma}}^{2} \tag{14b}$$

Explicitly, the interaction tensors $\tilde{\mathbf{M}}^{\alpha\beta}$ are written as:

$$\tilde{\mathbf{M}}^{11} = -\mathbf{V}^{1}:\mathbf{W}^{1}:\mathbf{M}^{(tg)} \tag{15a}$$

$$\tilde{\mathbf{M}}^{12} = \mathbf{V}^{1}:\mathbf{M}^{(tg)} \tag{15b}$$

$$\tilde{\mathbf{M}}^{22} = -\mathbf{V}^{2}:\mathbf{W}^{2}:\mathbf{M}^{(tg)} \tag{15c}$$

$$\tilde{\mathbf{M}}^{21} = \mathbf{V}^{2}:\mathbf{M}^{(tg)} \tag{15d}$$

where

$$\mathbf{V}^{1} = [(\mathbf{I} - \mathbf{T}^{2}:\mathbf{U}^{2}):[\mathbf{T}^{1}]^{-1}:(\mathbf{I} - \mathbf{T}^{1}:\mathbf{U}^{1}) - \mathbf{T}^{2}]^{-1} \tag{16a}$$

$$\mathbf{W}^{1} = (\mathbf{I} - \mathbf{T}^{2}:\mathbf{U}^{2}):[\mathbf{T}^{1}]^{-1} \tag{16b}$$

and where $\mathbf{V}^{2}$ and $\mathbf{W}^{2}$ can be obtained by interchanging indexes 1 and 2 in equations (16).

Using the secant microscopic relations for sites #1 and #2:

$$\underline{\dot{\epsilon}}^{1} = \mathbf{M}_{c}^{1(sec)}:\underline{\sigma}^{1} \tag{17a}$$

$$\underline{\dot{\epsilon}}^{2} = \mathbf{M}_{c}^{2(sec)}:\underline{\sigma}^{2} \tag{17b}$$

and the secant macroscopic relation [equation (10)] to remove the strain-rates from the interaction equations (14), we obtain a pair of *localization equations*:

$$\underline{\sigma}^{1} = \mathbf{B}_{c}^{1}:\underline{\Sigma} \tag{18a}$$

$$\underline{\sigma}^{2} = \mathbf{B}_{c}^{2}:\underline{\Sigma} \tag{18b}$$

where the location tensors $\mathbf{B}_{c}^{\alpha}$ are given by:

$$\mathbf{B}_{c}^{1} = \mathbf{F}_{c}^{1}:\mathbf{G}_{c}^{1} \tag{19a}$$

$$\mathbf{B}_{c}^{2} = \mathbf{F}_{c}^{2}:\mathbf{G}_{c}^{2} \tag{19b}$$

with

$$\mathbf{F}_{c}^{1} = \{(\mathbf{M}_{c}^{2(sec)} + \tilde{\mathbf{M}}^{22}):[\tilde{\mathbf{M}}^{12}]^{-1}:(\mathbf{M}_{c}^{1(sec)} + \tilde{\mathbf{M}}^{11}) - \tilde{\mathbf{M}}^{21}\}^{-1} \tag{20a}$$

$$\mathbf{G}_{c}^{1} = (\mathbf{M}_{c}^{2(sec)} + \tilde{\mathbf{M}}^{22}):[\tilde{\mathbf{M}}^{12}]^{-1}:(\mathbf{M}^{11} + \tilde{\mathbf{M}}^{12} + \mathbf{M}^{(sec)}) - (\mathbf{M}^{22} + \tilde{\mathbf{M}}^{21} + \mathbf{M}^{(sec)}) \tag{20b}$$

and where $\mathbf{F}_{c}^{2}$ and $\mathbf{G}_{c}^{2}$ can be obtained by interchanging indexes 1 and 2 in equations (20).

Using the connection between micro- and macro-stresses, i.e.

$$\underline{\Sigma} = \langle \underline{\sigma} \rangle \tag{21}$$

(where $\langle\ \rangle$ denotes a weighted average over both populations of grains) and taking an average of equations (18), we get the *self-consistent equation*:

$$\mathbf{M}^{(sec)} = \sum_{pairs} (\mathbf{M}_{c}^{1(sec)}:\mathbf{B}_{c}^{1})w_{c}^{1} + (\mathbf{M}_{c}^{2(sec)}:\mathbf{B}_{c}^{2})w_{c}^{2} = \langle \mathbf{M}_{c}^{1,2(sec)}:\mathbf{B}_{c}^{1,2} \rangle \tag{22}$$

where w_{c}^{1} and w_{c}^{2} are the volume fraction of site #1 and #2 of each pair with respect to the whole polycrystal. If all the grains in both phases have the same shape, the latter equation also guarantees that the micro–macro strain-rate connection also holds:

$$\underline{\dot{E}} = \langle \underline{\dot{\epsilon}} \rangle. \tag{23}$$

However, if the grains have different shape, the fulfilment of both closure conditions (21) and (23) requires that [16, 17]:

$$\mathbf{M}^{(sec)} = \langle \mathbf{M}_{c}^{1,2(sec)}:\mathbf{B}_{c}^{1,2} \rangle:\langle \mathbf{B}_{c}^{1,2} \rangle^{-1}. \tag{24}$$

If a given macroscopic strain-rate applied to the polycrystal $\underline{\dot{E}}^{(apl)}$ is known, the self-consistent scheme consists of choosing trial values for the local stresses (to get $\mathbf{M}_{c}^{\alpha(sec)}$, $\alpha = 1, 2$) and for the macroscopic compliance $\mathbf{M}^{(sec)}$. With the latter, Eshelby's ($\mathbf{S}^{\alpha\beta}$), interaction ($\tilde{\mathbf{M}}^{\alpha\beta}$) and localization ($\mathbf{B}_{c}^{\alpha}$) tensors can be calculated for each pair of sites. Next, equation (24) can be used iteratively to adjust the value of macroscopic compliance $\mathbf{M}^{(sec)}$ and the following

10×10 non-linear system can be solved to get an improved estimation for the local stresses:

$$\mathbf{M}_c^{1(sec)}(\underline{\boldsymbol{\sigma}}):\underline{\boldsymbol{\sigma}}^1 - \underline{\dot{\mathbf{E}}} = (\tilde{\mathbf{M}}^{11} + \tilde{\mathbf{M}}^{12}):([\mathbf{M}^{(sec)}]^{-1}:\underline{\dot{\mathbf{E}}}^{(apl)}) - \tilde{\mathbf{M}}^{11}:\underline{\boldsymbol{\sigma}}^1 - \tilde{\mathbf{M}}^{12}:\underline{\boldsymbol{\sigma}}^2 \quad (25a)$$

$$\mathbf{M}_c^{2(sec)}(\underline{\boldsymbol{\sigma}}):\underline{\boldsymbol{\sigma}}^2 - \underline{\dot{\mathbf{E}}} = (\tilde{\mathbf{M}}^{21} + \tilde{\mathbf{M}}^{22}):([\mathbf{M}^{(sec)}]^{-1}:\underline{\dot{\mathbf{E}}}^{(apl)}) - \tilde{\mathbf{M}}^{21}:\underline{\boldsymbol{\sigma}}^1 - \tilde{\mathbf{M}}^{22}:\underline{\boldsymbol{\sigma}}^2 \quad (25b)$$

After reaching convergence, the crystallographic orientation of each site is updated according to the total lattice rotation-rates:

$$\underline{\dot{\boldsymbol{\omega}}}^1 = \underline{\dot{\boldsymbol{\Omega}}} - \underline{\dot{\boldsymbol{\omega}}}^{1(pl)} + \underline{\tilde{\boldsymbol{\omega}}}^1 \quad (26a)$$

$$\underline{\dot{\boldsymbol{\omega}}}^2 = \underline{\dot{\boldsymbol{\Omega}}} - \underline{\dot{\boldsymbol{\omega}}}^{2(pl)} + \underline{\tilde{\boldsymbol{\omega}}}^2 \quad (26b)$$

where $\underline{\dot{\boldsymbol{\Omega}}}$ is the macroscopic rotation-rate, $\underline{\dot{\boldsymbol{\omega}}}^{\alpha(pl)}$ are the plastic rotation-rates and $\underline{\tilde{\boldsymbol{\omega}}}^{\alpha}$ are the local rotations-rates, calculated as

$$\underline{\tilde{\boldsymbol{\omega}}}^1 = \mathbf{Y}^{11}:\underline{\tilde{\boldsymbol{\epsilon}}}^1 + \mathbf{Y}^{12}:\underline{\tilde{\boldsymbol{\epsilon}}}^2 \quad (27a)$$

$$\underline{\tilde{\boldsymbol{\omega}}}^2 = \mathbf{Y}^{21}:\underline{\tilde{\boldsymbol{\epsilon}}}^1 + \mathbf{Y}^{22}:\underline{\tilde{\boldsymbol{\epsilon}}}^2. \quad (27b)$$

The $\mathbf{Y}^{\alpha\beta}$ tensors are defined as

$$\mathbf{Y}^{11} = \boldsymbol{\Pi}^{11}:\mathbf{T}^1:\mathbf{U}^1 - \boldsymbol{\Pi}^{12}:\mathbf{T}^2 \quad (28a)$$

$$\mathbf{Y}^{12} = \boldsymbol{\Pi}^{12}:\mathbf{T}^2:\mathbf{U}^2 - \boldsymbol{\Pi}^{11}:\mathbf{T}^1 \quad (28b)$$

where, complementary to equation (4), the skew-symmetric Eshelby tensors $\boldsymbol{\Pi}^{\alpha\beta}$ are defined as

$$\boldsymbol{\Pi}^{\alpha\beta} = \text{skewsym}(\boldsymbol{\Gamma}^{\alpha\beta}):\mathbf{L} \quad (29)$$

and where $\mathbf{Y}^{21}$ and $\mathbf{Y}^{22}$ can be obtained by interchanging indexes 1 and 2 in equations (28).

3. APPLICATION

In this section, the VPSC-2S model is used to predict the texture evolution of two-phase titanium-based alloys. These $(\alpha + \beta)$ Ti alloys have found several technological applications and therefore their microstructure and texture were intensively investigated. Depending on the previous thermomechanical treatments, these alloys exhibit two different kind of microstructures, i.e. globular and lamellar [18–20]. While in the former case, the grains of both phases are approximately equiaxed and there is no correlation between the orientations of two neighbour α- and β-grains, in the latter very elongated α-grains grow inside initially large β-grains. The final structure consists of elongated α- and β-grains (lamellae) which orientations are correlated by means of the Burgers relationship [20]:

$$(0001)_\alpha // \{110\}_\beta \quad (30a)$$

$$\langle 1\bar{2}10\rangle_\alpha // \langle 111\rangle_\beta \quad (30b)$$

from where other relationships follow:

$$\{10\bar{1}0\}_\alpha // \{112\}_\beta \quad (31a)$$

$$\langle 1\bar{2}10\rangle_\alpha // \langle 111\rangle_\beta. \quad (31b)$$

Moreover, the habit plane between phases is given by $\{5\bar{1}\bar{4}0\}_\alpha$, near to $\{10\bar{1}0\}_\alpha$ [20]. The existence of these strong correlations in orientation and morphology between α- and β-grains in lamellar structures should give a non-negligible influence of the neighbourhoods on the local plastic behaviour of each phase. Therefore, the texture evolution of these lamellar structures appears as a challenging bench case to test the validity of the VPSC-2S model. In fact, the texture evolution of Ti–Al–V alloys has been widely reported by Mecking and co-authors for different structures, phase fractions and temperatures [18, 19, 21–24]. In the specific case of lamellar structures with low β-content (e.g. around 20%) heavily rolled at high temperature, the texture of the α-phase shows a strong $\{1\bar{2}10\}\langle 10\bar{1}0\rangle$ component which gives a basal maximum in the transverse direction (TD) [21–24]. On the other hand, for similar β-content, temperature and loading path, the globular structure develops a rather smooth $\{hkil\}\langle 10\bar{1}0\rangle$ fibre [21–24].

In what follows, we use the VPSC-2S to show how the main features of the α-texture of a lamellar material can be ascribed to the vicinity effects which arise from the existing correlations in orientation and morphology between phases. Figure 1 shows five different calculated basal pole figures. All of them were obtained by assuming:

(a) 20% β-content;
(b) rolling up to 1.2 true strain;
(c) initial morphology for α-grains, 2.0:1.0:0.2 (ellipsoid's radii) and for β-grains, 2.0:1.0:0.05. The ellipsoids are tangent and they are aligned along their short axes (therefore the distance between centres is 0.25). The initial morphologic texture (i.e. the spatial orientation of the ellipsoids) is random;
(d) the active slip modes in the β-phase are $\{1\bar{1}0\}\langle 111\rangle$ slip and $\{11\bar{2}\}\langle 111\rangle$ slip. The initial CRSS of both β-phase slip modes is 0.25 (arbitrary units). For the α-phase, the active slip modes are the prismatic $\{10\bar{1}0\}\langle 1\bar{2}10\rangle$ slip and basal $(0001)\langle 1\bar{2}10\rangle$ which are assumed to be four times harder than the β-phase modes (the initial CRSS of both $\langle a\rangle$-modes is 1.0) and the pyramidal $\langle c + a\rangle$ $\{10\bar{1}1\}\langle 1\bar{2}13\rangle$ slip which is assumed to be eight times harder than the prismatic and basal modes (the initial CRSS of pyramidal $\langle c + a\rangle$ is 8.0 in the same units);
(e) homotetic hardening, i.e. the relative CRSS do not change as deformation proceeds;
(f) viscoplastic exponent $n = 5$.

In order to compare both models, the first two cases were obtained using the 1-site approach [6] while the last three cases are 2-site simulations. The five simulations were performed by assuming an

initial random texture of 400 grains of each phase but different correlations in orientation and morphology were assumed in each case. Cases (a) and (c) correspond to non-correlated α- and β-textures, i.e. 400 ($\alpha + \beta$) pairs were formed by choosing randomly 400 α-phase and 400 β-phase crystallographic orientations and an arbitrary morphologic orientation (orientation of the ellipsoid's principal axes) was assigned to each pair. On the other hand, the initial configuration for cases (b) and (e)—labelled "full correlation"—was built as follows: (1) 400 α-orientations were randomly selected; (2) from each α-orientation, a β-orientation was obtained to form the pair by using the Burgers relationship (a random variant selection among the 12 possible choices was performed); (3) the morphologic orientation was selected so as to align the short axes of the ellipsoids (i.e. the habit plane's normal) with a $\{10\bar{1}0\}$ α plane. Case (d) is an intermediate case: the β-orientations were determined from the α-ones but the morphologic orientation of each pair of grains was randomly selected giving, in crystal axes, a random orientation of the habit plane. For the latter initial configuration, only the 2S result is reported provided the 1S approach is insensitive to crystallographic correlations and it would give the same results as case (a).

Although the simulation was carried out assuming an initial morphology of flat grains, the 1S non-correlated texture [case (a), Fig. 1(a)] resembles the experimental textures measured in globular materials. This result is expected since the non-correlated configuration is compatible with the globular material and the initial existence of flat grains just speeds up the grain shape effect which will appear in the actual globular case. Remaining within the 1S approach, but when the full correlation is considered [case (b), Fig 1(b)] a slight tendency of the basal poles towards TD can be observed but the $\{hkil\}\langle 10\bar{1}0\rangle$ fibre is still the main feature of the predicted texture. In this case, although the initial correlations were adequate, the model itself is unable to account for the vicinity effects which may affect the texture formation.

If the VPSC-2S model is used in the non-correlated case [case (c), Fig. 1(c)] the results are not very different from the 1S approach. In this case, provided the pairs of interacting grains were randomly selected, the overall neighbour effect is cancelled. When the crystallographic correlation (but not the morphologic one) is taken into account the results are not improved [case (d), Fig 1(d)] showing that the orientation of the habit plane may also be relevant (and not only the Burgers relationship, as considered

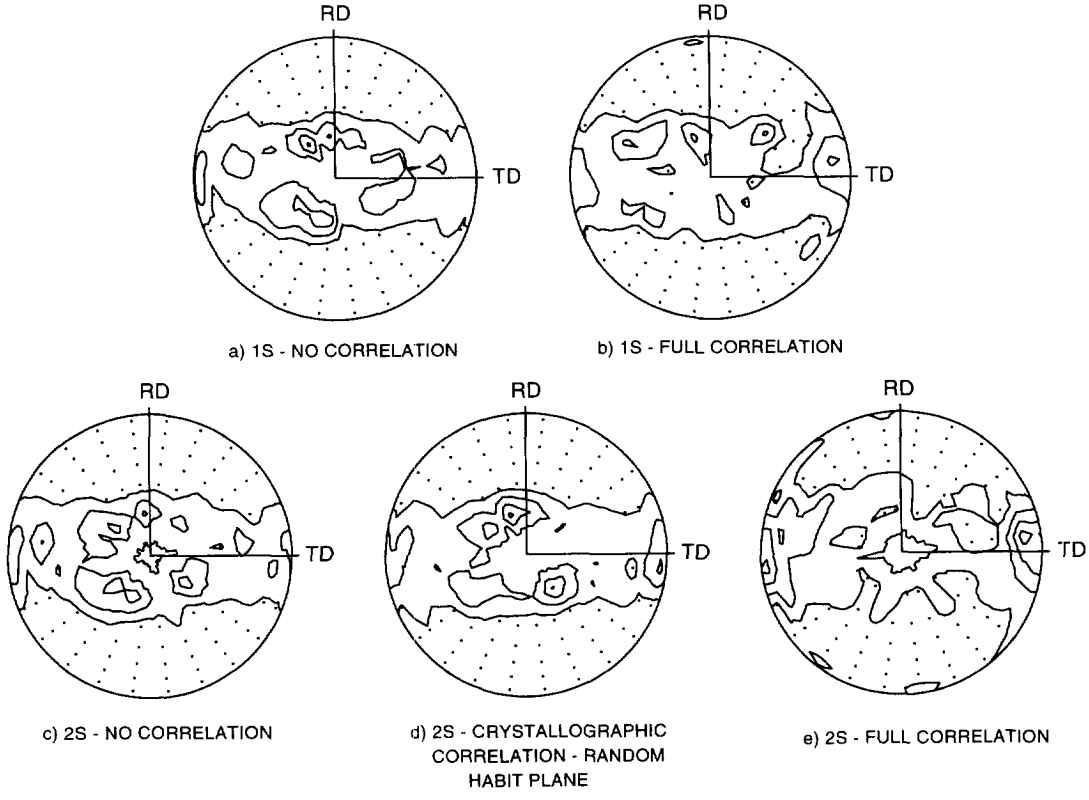

Fig. 1. 1-site and 2-site calculated α-textures (basal poles figures) of a lamellar ($\alpha + \beta$) Ti-alloy with 20% of β-content, rolled up to 1.2 true strain, assuming different morphologic and crystallographic correlations between phases. Lines are multiples of random distribution (mrd). Dots are orientations below 1 mrd.

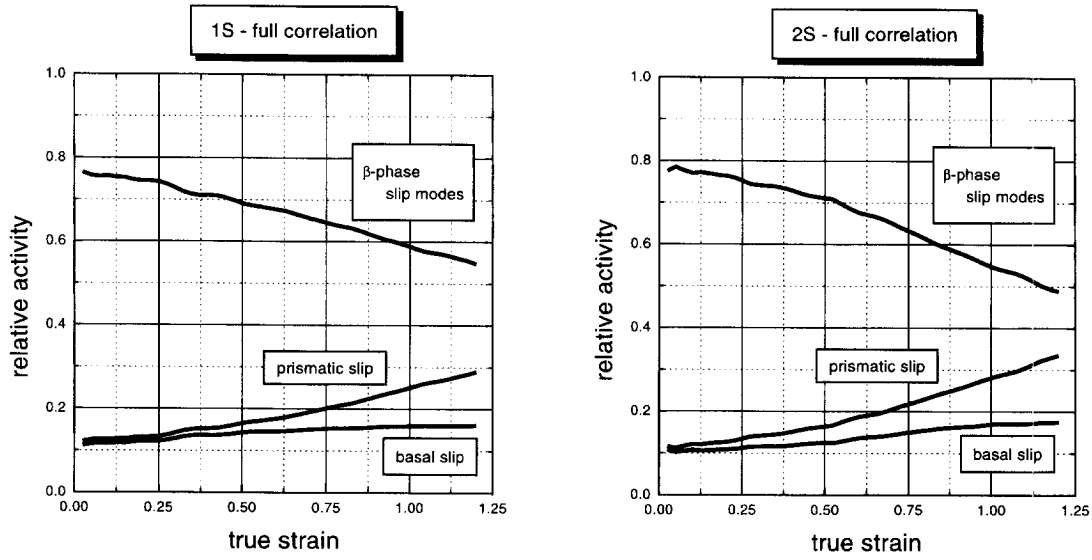

Fig. 2. Relative activity of both β-phase slip modes and prismatic and basal α-phase slip modes, calculated with the 1-site and 2-site viscoplastic models, considering full correlation between phases.

in Ref. [21]). In fact, only the 2S fully correlated simulation [case (e), Fig. 1(e)] shows the appearance of the basal maximum in TD. We can therefore conclude that the mean feature of the texture of a lamellar material (i.e. the basal maximum in TD) is well reproduced by the VPSC-2S model when the actual correlations between phases are properly taken into account.

It is also revealing to regard how both phases share the applied strain. Figure 2 shows the relative activity of the different α- and β-slip modes as a function of the accumulated strain, predicted by the 1S and 2S models for the fully correlated case [cases (c) and (e), respectively]. In both cases, most of the deformation is carried by the softer β-phase (the global contribution of both β-slip modes is plotted: each of them accommodates half of the total strain of the β-phase). The β-phase slip activity starts at around 80% and decreases as deformation proceeds. In the α-phase, the activity of the prismatic slip increases faster than the basal slip. Hence, provided the main difference between the 1S and the 2S cases is given by a higher contribution of the prismatic slip with detriment to the β-phase activity, it can be stated that:

(a) the formation of the basal maximum in TD can be ascribed to this higher prismatic activity, as proved in Ref. [25] for a single-phase hcp material;
(b) the correlations between the α- and β-grains favour the prismatic activity in the α-phase. As can be seen from the relationships (27) and (28), each pair of normal and Burgers vectors of the $\{10\bar{1}0\}\langle 1\bar{2}10\rangle$ prismatic slip mode in the α-phase is parallel to another pair of normal and Burgers vectors of the $\{11\bar{2}\}\langle 111\rangle$ slip mode in the β-phase. Moreover, one of the prismatic slip systems in each α-grain is almost parallel to the habit plane. Therefore, the simultaneous activation in each phase of these "parallel" slip systems [20] may minimize the discontinuity of the distortion across the habit plane, which is a sound condition when the interaction between neighbours is taken into account.

Finally, we will discuss the VPSC-2S predictions for the β-texture. Although most of the deformation is carried by the softer b.c.c. phase, we will show that the severity of the β-texture is controlled by the grain shape effect. Figure 3 shows predicted α- and β-textures (basal and $\{110\}$ pole figures, respectively) for two different initial shapes and updating criteria of the β-grains. Case (a) in Fig. 3 is identical to case (e) in Fig. 1 (i.e. the initial grain shapes are 2.0:1.0:0.2 for α-grains and 2.0:1.0:0.05 for β-grains) while case (b) was obtained by assuming more rounded β-grains (but keeping the relative volume, i.e. 1.25:0.8:0.1 for β-grains) and preventing the grain shape updating of the β-phase. The latter condition can be justified by regarding that the soft phase actually flows around the hard grains. Consequently, there is only an "effective" portion of the β-grains which keeps the correlations with the α-phase. The long axis of the effective β-grain would be approximately as large as the one of the neighbour α-grains. On the other hand, if this is the actual behaviour of the β-phase, we are aware that the VPSC approach fails to describe the behaviour of those β-regions which flow around the hard phase.

In the first case, the predicted β-texture is rather smooth: it reaches a maximum of 2 mrd (multiple of

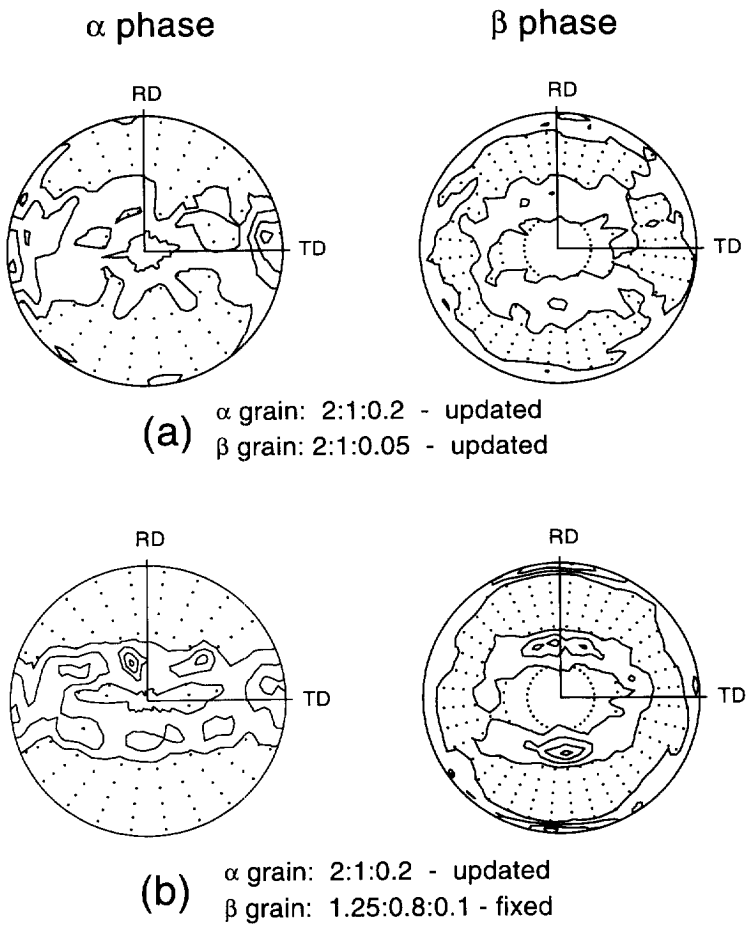

Fig. 3. α- and β-textures [basal and (110) poles figures, respectively] calculated with the VPSC-2S (full correlation case) of a lamellar ($\alpha + \beta$) Ti-alloy with 20% β-content, rolled up to 1.2 true strain, assuming different initial shapes and updating criteria for the β-grains. Lines are multiples of random distribution (mrd). Dots are orientations below 1 mrd.

random distribution). This result is due to a strong grain shape effect: flat β-grains have associated high local rotations [see equations (27)] which tend to align their long grain axes with the normal direction (ND) and their short axes with the rolling direction (RD) and therefore determine a high reorientation rate that prevents the formation of strong stable texture components. On the other hand, when the β-grains are assumed to be more rounded and their shape is kept fixed throughout the calculation, the relative magnitude of the local rotation decreases and allows the formation of a maximum of around 4 mrd. Nevertheless, although this is approximately the severity measured for a β-texture under similar conditions [23, 24], the main component of the latter, i.e. a partial $\{111\}\langle hkl\rangle$ fibre, does not match with the experimental results which give a mean texture component in $\{001\}\langle 110\rangle$. As stated earlier, these disagreements may be due to the lack of an accurate description of the flow of part of the β-grains around the harder α-regions.

4. CONCLUSIONS

This work shows that the correlation between phases in a two-phase material has a strong influence on texture formation. In the case of ($\alpha + \beta$) Ti-alloys, the VPSC-2S calculations make it evident that the Burgers relationship together with orientation of the habit plane contributes to an increase of the relative activity of the prismatic slip which is known to be associated with the formation of a TD maximum of the α-texture. The β-texture formation, however, cannot be fully explained by means of the present model. This disagreement can be ascribed to the flow of the β-phase around the α-regions, an effect that the present model cannot account for.

On the modelling side, a comprehensive description of the VPSC-2S model has been accomplished using the Eshelby–Hill formulation. Further applications of this 2-site approach, conceived to account for neighbour effects in the frame of homogenization methods, are currently being developed for materials under different deformation regimes, e.g. a 2-site

elastoplastic model to treat damaged Al-alloys [26] and a 2-site linear viscous model to describe the under-irradiation behaviour of ($\alpha + \beta$) Zr-alloys [27].

Acknowledgements—We wish to thank Prof. H. Mecking and Dr D. Dunst for fruitful discussions. One of the authors (R.L.) wishes to acknowledge Région Rhône-Alpes for financial support during his stay at GPM2 Laboratory during 1995. Close collaboration between IFIR and GPM2 is also possible through a CNRS-CONICET agreement.

REFERENCES

1. Sachs, G., *Z. Verein. Deutch Ing.*, 1928, **72,** 734.
2. Taylor, G. I., *J. Int. Metals*, 1938, **62,** 307.
3. Hutchinson, J. W., *Proc. R. Soc. London*, 1970, **A319,** 247.
4. Hutchinson, J. W., *Proc. R. Soc. London*, 1976, **A348,** 101.
5. Molinari, A., Canova, G. R. and Ahzi, S., *Acta metall.*, 1987, **35,** 2983.
6. Lebensohn, R. A. and Tomé, C. N., *Acta metall. mater.*, 1993, **41,** 2611.
7. Zeller, R. and Dederichs, P. H., *Physica status solidi* (b), 1973, **55,** 831.
8. Eshelby, J. D., *Proc. R. Soc. London*, 1957, **A241,** 376.
9. Hill, R., *J. Mech. Phys. Solids*, 1965, **13,** 89.
10. Honneff, H. and Mecking, H., *Proc. Sixth Int. Conf. on Texture of Materials* (ICOTOM-6), ed. S. Nagashima. Iron and Staal Inst. Japan, Tokyo, 1981, p. 347.
11. Canova, G. R., Kocks, U. F. and Jonas, J. J., *Acta metall.*, 1984, **32,** 211.
12. Tiem, S., Berveiller, M. and Canova, G. R., *Acta metall.*, 1986, **34,** 2134.
13. Canova, G. R., Wenk, H. R. and Molinari, A., *Acta metall. mater.*, 1992, **40,** 1519.
14. Mura, T., *Micromechanics of Defects in Solids*. Martinus-Nijhoff, Dordrecht, 1988.
15. Berveiller, M., Fassi-Fehri, O. and Hihi, A., *Int. J. Engng Sci.*, 1987, **25,** 691.
16. Walpole, L. J., *J. Mech. Phys. Solids*, 1969, **17,** 235.
17. Lebensohn, R. A., Solas, D., Canova, G. R. and Brechet, Y., *Acta mater.*, 1996, **44,** 315.
18. Morii, K., Mecking, H. and Lütjering, G., *Proc. 7th Int. Conf. on Strength of Metals and Alloys*, ed. H. J. McQueen *et al.* Pergamon Press, Oxford, 1985, p. 251.
19. Morii, K., Mecking, H., Lütjering, G. and Nakayama, Y., *Scripta metall.*, 1986, **20,** 1795.
20. Ankem, S. and Margolin, H., *Metall. Trans. A*, 1986, **17A,** 2209.
21. Bacroix, B., Canova, G. R. and Mecking, H., *Proc. MECAMAT '91*, ed. C. Teodosiu and J. L. Raphanel. Balkema, Rotterdam, p. 101.
22. Dunst, D., Dendievel, R. and Mecking, H., *Mater. Sci. Forum*, 1994, **157–162,** 665.
23. Dunst, D., PhD. Thesis, Technische Universität Hamburg, Germany, 1995.
24. Dunst, D. and Mecking, H., *Z. Metallk.*, 1996, **87,** 506.
25. Lebensohn, R. A., PhD. Thesis, Universidad Nacional de Rosario, Argentina, 1993.
26. Solas, D., Lebensohn, R. A. and Canova, G. R., to be published.
27. Canova, G. R. and Tomé, C. N., to be published.

APPENDIX

The integrals for the calculation of $\Gamma^{\alpha\beta}$ are derived from the solution of the equilibrium equation inside both interacting inclusions using the Fourier transform of Green's functions technique (for details, see Bervellier *et al.* [15]). For example, Γ^{12} (in main axes of site 1) can be calculated as:

$$\Gamma^{12}_{ijmn} = -\frac{3}{2\pi^2}(a_2 b_2 c_2)\int_0^{\pi}\int_0^{2\pi} \times \frac{\alpha_m \alpha_j K^{-1}_{ni} \sin\theta F(\theta, \varphi)}{\rho_1^3 \rho_2^3}\, d\varphi\, d\theta \quad (A.1)$$

with

$$\bar{\alpha} = (\sin\theta\cos\varphi,\ \sin\theta\sin\varphi,\ \cos\theta) \quad (A2)$$

$$K^{-1}_{ik} = [L_{ijkl}\alpha_j\alpha_l]^{-1} \quad (A.3)$$

$$\bar{\rho}_1 = (a_1\alpha_1,\ b_1\alpha_2,\ c_1\alpha_3) \quad (A.4)$$

$$\bar{\rho}_2 = (a_2\psi_{1j}\alpha_j,\ b_2\psi_{2j}\alpha_j,\ c_2\psi_{3j}\alpha_j)$$

$$F(\theta,\varphi) = \frac{1}{24}(-\lambda^3 + 3\rho_2\lambda^2 + 3\rho_1\lambda^2 - 6\rho_1\rho_2\lambda)\ \frac{\pi}{2}\,\mathrm{sgn}(\lambda)$$

$$+\frac{1}{24}(\beta^3 - 3\rho_2\beta^2 + 3\rho_1\beta^2 - 6\rho_1\rho_2\beta)\ \frac{\pi}{2}\,\mathrm{sgn}(\beta)$$

$$+\frac{1}{24}(\gamma^3 + 3\rho_2\gamma^2 - 3\rho_1\gamma^2 - 6\rho_1\rho_2\gamma)\ \frac{\pi}{2}\,\mathrm{sgn}(\gamma)$$

$$+\frac{1}{24}(-\delta^3 + 3\rho_2\delta^2 + 3\rho_1\delta^2 - 6\rho_1\rho_2\delta)\ \frac{\pi}{2}\,\mathrm{sgn}(\delta). \quad (A.5)$$

In equation (A.1)–(A.5), (a_1, b_1, c_1) and (a_2, b_2, c_2) are the radii of the ellipsoids in sites #1 and #2, ψ_{ij} is the transformation matrix from main axes of site 2 to main axes of site 1 and

$$\lambda = \rho_1 + \rho_2 - c$$

$$\beta = \rho_2 + c - \rho_1$$

$$\gamma = c + \rho_1 - \rho_2$$

$$\delta = \rho_1 + \rho_2 + c$$

with

$$\bar{c} = \bar{\alpha} \times \bar{\mathbf{R}}_0,$$

where $\bar{\mathbf{R}}_0$ is the vector from the centre of site 1 to the centre of site 2.